ISSN: 0067-2904

# Dielectric and gas sensing properties of *in situ* electrochemically polymerized PPy-MgO-WO3 nanocomposite films

**Yahya M. Abbas*, Ahmed Abbas**
[1]Science Department, College of Basic Education, Wasit University, Wasit, Iraq
[2]Physics Department, College of Science, University of Baghdad, Baghdad, Iraq

Received: 20/9/2020 Accepted: 18/12/2020

**Abstract**

A polypyrrole-based ammonia-detection gas sensor was studied in this work. Under a 1.6 V electrodeposition potential, polypyrrole (PPy) was electrochemically synthesized from an aqueous solution of 0.1 M pyrrole and 0.1 M oxalic acid. An extension to the polypyrrole films was applied through electrochemical deposition on indium tin oxide (ITO), using the metal oxide nanoparticles of MgO and $WO_3$. These films were investigated for their sensing behavior towards $NH_3$ at different working temperatures and different weight percentages of nanoparticles .The measurements of A.C conductivity were conducted over a frequency range of $10^1$-$10^5$ Hz and temperature range of 298-423 K . The highest electrical conductivity was equal to $3.67x10^{-1}$ $\Omega.cm^{-1}$ at a temperature of 323 K and frequency of $10^5$H z. The experimental results showed that the sensitivity of the undoped and doped PPy with nanoparticle films to ammonia gas changes with the change in temperature and weight percentage.

**Keywords:** Ammonia, Polypyrrole, Nanoparticles, ElectroChemical Polymerization, Gas sensor

# خصائص العزل الكهربائي و تحسسية الغازات للمتراكبات النانونية لاغشيةPPy:MgO,WO3 المحضرة بطريقة البلمرة الكهروكيميائية الموقعية المتزامنة

**يحيى منعم عباس*، احمد عباس**
[1] قسم العلوم, كلية التربية الاساسية, جامعة واسط, واسط, العراق
[2] قسم الفيزياء, كلية العلوم, جامعة بغداد, بغداد, العراق

**الخلاصة**

في هذا العمل تم دراسة متحسس للكشف عن غاز الأمونيا يعتمد على البولي بايرول . باستخدام فرق جهد 1.6 فولت للترسيب الكهربائي تم بلمرة البولي بيرول كهروكميائيًا باستخدام 0.1M من محلول بايرول مائي و 0.1M حامض أوكزالك اسيد. اغشية البولي بيرول رسبت بطريقة كهروكيميائية على أكسيد قصدير انديوم ITO وتم استخدام اكاسيد المعادن النانوية MgO و WO3 كمضافات لهذه الاغشية. تم فحص سلوك تحسسية هذه الأغشية اتجاه غاز NH3 في درجات حرارة عمل مختلفة ونسبة وزنية مختلفة من الجسيمات النانوية المضافة. تم إجراء قياسات التوصلية الكهربائية ضمن مدى تردد ($10^1$ – $10^5$هرتز) ومدى درجة الحرارة (298–423 ) كلفن. اظهرت النتائج اعلى توصلية كهربائية عند التردد $10^5$ هرتز و درجة حرارة

*Email: yamuab6@gmail.com

323 كلفن تساوي $3.67x\ 10^{-1}(\Omega.cm)^{-1}$ ، كذلك أظهرت النتائج التجريبية ان حساسية البولي بايرول غير المطعم والمطعم بجسيمات نانوية لغاز الأمونيا تتغير مع التغير في درجة الحرارة وتغير النسب المئوية لوزن المضافات النانوية.

## 1-Introduction

Typically, conducting polymers can be synthesized by oxidizing the corresponding monomers chemically or electrochemically. The electrochemical method of synthesizing a standard conducting polymer, i.e. electrochemical deposition, is the most effective way of depositing conductive polymers (CPs) in films. During the increasing phase of the film, the film's thickness can be controlled by the total charge passed through the electrochemical cell. Additionally, the film can be deposited on patterned microelectrodes [1]. Polypyrrole is a type of organic polymers that is formed by petroleum polymerization. It was first demonstrated to be a conducting polymer in 1968 [2]. Due to its simple deposition from aqueous and non-aqueous media, its adherence to several types of substrates, its high electrical conductivity and its stability in air and aqueous media, PPy remains one of the most studied among the various conducting polymers. The simplicity of planning and the probability of electrochemical regulation of experimental conditions make it the most employed way [3]. PPy has an oxidized stabilized form, towering conductivity, water solubility, commercially availability, and useful electrical and optical properties [4]. Due to their activity at room temperature and easy processing of sensor components, polymers such as PPy and polyaniline have been studied as sensing materials in recent years [5, 6]. A sensor is a device which can be used for translating an input parameter into a signal. The sensor's output signal is typically based on alterations in electrical or optical properties. CPs exhibit reversible variations in conductivity, colour , and thickness, making them ideal sensing materials. Since CPs may interact with organic compounds and moisture present in the surrounding environment, they are often unstable and thus can exhibit low sensitivity and selectivity to a target analyte that requires improvement. Many attempts have been made to boost the sensitivity and selectiveness of CP sensors by tailoring their properties [7]. Forzani *et al*. [8] developed a chemical sensor based on both amperometric and conductometric modes. Ammonia is commonly used in many applications, including chemical industries, e.g. the manufacture of nitric acids, petrochemical industries, industrial hygiene testing, and environmental pollution control of calibration gas mixtures. Ammonia, however, is among a category of highly toxic gases that, if exposed, cause hazards to the respiratory systems, eyes and skin. Ammonia is water-soluble, where it hydrolyzes to ammonium hydroxide, a solid base that irritates the upper respiratory tract and skin. It is therefore important to have sensors that can detect ammonia at room temperature at a very low level (few ppms). Recent studies identified PPy for ammonia sensing applications, synthesized by electrochemical [6] and Langmuir–Blodgett technique [9]. Currently, the use of nanocomposites made of conducting polymers and metal oxides for gas sensing applications has attracted considerable interest. It has been shown that hybridization can synergize or complement the sensitive properties of pure organic or inorganic gas sensing materials [10]. Kwon *et al*.[11] investigated the impact of PPy nanoparticle size on chemical sensing behaviors when detecting volatile organic compounds and toxic gases to improve the efficiency of CPs in chemical sensors. The conductivity and surface-to - volume ratio were found to have increased with decreasing sizes of nanoparticles. Based on the smallest PPy nanoparticles (20 nm), the chemical sensor showed the best sensing efficiency, i.e. excellent sensitivity, quick response time, reversibility and reproducible responses. Many metal oxides have finite band gap energies that can be paired with CP ones. As a consequence, the judicious application of metal oxides can modulate the electrical electronic properties of CPs, which also allow for specific mechanisms of chemical-electrical transduction. In addition , metal oxides can be readily incorporated into CPs as nanostructures, leading to enhanced surface areas [12]. In this paper, we address the $NH_3$ sensing properties of chemically (*in situ*) deposited undoped polypyrrole and that doped with tungsten and magnesium oxide thin films of nanoparticles with different concentrations at different temperatures and quick response time.

## 2-Theoritical part

The total conductivity ($\sigma_t$ (ω)) at a given frequency (ω) is a contribution of two parts, which are the conductivity of $\sigma_{d.c}$ at low frequency and the conductivity of $\sigma_{a.c}$ (ω)due to relaxation processes [13], as follows:

$$\sigma_t(\omega) = \sigma_{a.c}(\omega) + \sigma_{d.c} \quad \text{or} \quad \sigma_t(\omega) = A\omega^s + \sigma_{d.c} \tag{1}$$

where (s) is a function of frequency and is determined from the slope of the plot $\ln \sigma_{a.c}(\omega)$ versus $\ln(\omega)$, then [14]:

$$s = \frac{d[Ln\sigma_{a.c}(\omega)]}{d[Ln(\omega)]} \tag{2}$$

The frequency-dependent conductivity ($\sigma_t$ (ω)) part reveals three regions; region (a) which is due to the electrodes polarization effect , region (b) which is related to $\sigma_{d.c}$ , and region (c) at high frequency, which is related to $\sigma_{a.c}$ (ω). In this region, $\sigma_{a.c}$(ω) is proportional to $\omega^s$. The frequency-dependent a.c conductivity ($\sigma_{a.c}$ (ω)) is ascribed to three mechanisms of carriers transport [ 15 , 16]; (1) excitation and transporting of charge carriers to the extended state near conduction or valence bands V.B, thus $\sigma_{a.c}$ (w) is given by:

$$\sigma_{a.c}(\omega) = \sigma_0 / (1+\omega^2\tau) \tag{3}$$

where $\sigma_0 = ne^2\tau/m^*$ and m*, n, and e are the electron effective mass, charge carrier density, and electron charge, respectively; (2) excitation and transporting of charge carriers into localized states at the edges of the valence or conduction bands. $\sigma_{a.c}$ (ω) obeys the equation:

$$\sigma_{a.c}(\omega)\ \alpha\omega\ [1n(1\backslash\omega\tau)]^4 \tag{4}$$

where $\omega<1/\tau$ ; (3) transporting by hopping of charge carriers near the Fermi level, thus $\sigma_{a.c}$(ω) obeys the equation [17]:

$$\sigma_{a.c}(\omega) = 1/3\ \pi e^2 k_B T\ [N(E_F)]^2\ \bar{\alpha}^{-5}\omega\ [1n(1/\omega\tau)]^4 \tag{5}$$

where $N(E_F)$ , α are the density of state near Fermi level and the decay factor $\bar{\alpha}^{-1} = r_p$, where $r_p$ is polaron radius.

Various theories were postulated to explain a.c conduction. These theories usually suppose that the dielectric loss happens due to the motion of charge carriers which are localized within the pairs of sets. Two discrete processes were postulated. The first is the quantum mechanical tunneling (QMT), in which the a.c conductivity is linearly dependent on temperature and the exponent s is frequency-dependent , whereas it is independent on temperature [16]. The second process is the correlated barrier hopping (CBH) . In this process, when the electrons hope over the potential barrier between two sites, the a.c conductivity is due to hopping between defect states or dangling bonds ($D^+$ $D^-$) . In the case of the CBH, $\sigma_{a.c}$(ω) is exponentially dependent on temperature, and the exponent **s** approaches unity when the temperature approaches zero [13].

The dielectric constant (εr), dielectric loss (εi), and a.c conductivity (σ*ac*) of the samples are estimated by applying the following relations [ 18]:

$\varepsilon_r = (d/\varepsilon_o A)C$ (6)

$\varepsilon_i = \varepsilon_r(\tan\delta)$ (7)

$\sigma_{a.c} = \omega\varepsilon_o\varepsilon$ (8)

where c , d, and a are the capacitance, the thickness, and the area of the sample, respectively .

The sensor's response to reducing gas, such as methanol, ammonia, and hydrogen $H_2S$ is detected through the sensors resistance, where the sensitivity is given by [19, 20]:

$S = ((Rg - Ra) / Ra) \times 100\%$ (9) if $Rg > Ra$

$S = ((Ra - Rg) / Ra) \times 100\%$ (10) if $Ra > Rg$

where Ra and Rg are the resistance values of the sensor film in clean air and in the measuring gas, respectively .

Response time ($t_{res}$) refers to the time needed to reach a stable sensor response after a stepwise increase in the stimulus. Usually, the response time is defined as the time 90%, i.e. the time it takes for 90% change in the sensor response after an increase in the stimulus is accomplished Recovery time ($t_{rec}$) refers to the time the sensor needs to resume zero response after removing the stimulus, i.e. the time a sensor needs to recover from the effect of the precedent stimulus. $t_{rec}$ is the time needed for 90%

change in the sensor response after stimulus removal is accomplished [21]. Thus the response and the recovery times are calculated by applying the following equations:

$T_{res}=R_{air}-90\%(R_{air}-R_{gas})$

$T_{rec}= R_{air}+90\%(R_{air}-R_{gas})$

## 3 -Experimental protocols

### 3 -1 Materials

A suitable solution for the electropolymerization of PPy was prepared using 0.1 M of pyrrole monomer doped with oxalic acid (0.1 M) and oxidized with 150 ml of distilled water. In all cases, an electrochemical double-electrode cell was used .The working electrode was an indium-doped tin oxide (ITO) (4 $cm^2$) and the counter-electrode was a sheet of platinum (6 $cm^2$). Both electrochemical experiments were performed at R.T (298 K). Pyrrole was purchased from Cheng Du Micxy Chemical Co. (article 161208002, 98 percent pure). Oxalic acid was purchased from BHD Chemical Ltd.The nanoparticles of MgO and $WO_3$ were used as doping agents.

### 3-2 PPy Synthesis

In 150 mL of distilled water, 1.35 g of oxalic acid ($C_2H_2O_4$) was added and stirred for around 5 minutes until it was fully dissolved and a clear aqueous solution was obtained. After stirring for around 5 minutes, 1.036 mL of pyrrole monomer was added dropwise into the solution. After obtaining the mixture of aqueous oxalic acid solution, nanoparticles (MgO and $WO_3$) were added as doping materials in different concentrations (0.01, 0.03, and 0.05). Ultrasonic waves were used to homogenize the nanoparticles with the solution. The monomer potential (1.6V) was applied by the power supply between the ITO and the platinum for around 5 minutes with continuous stirring until the polymerization is complete. The pure black PPy and the doped precipitated film were applied on the ITO glass substrate. The results of studying the dielectric properties were obtained using a GW Instek 100kHz High Precision LCR Meter (LCR-6100, Taiwan).

## 4- Results and discussion

Figures-(1, 2, and 3) show the relation between Ln(σ) versus Ln(ω) for the pure PPy and ppy/(MgO and $WO_3$) nanoparticle blends. It is clearly observed that the conductivity is frequency-independent in the low frequency range, i.e. 10-60 Hz, but becomes frequency-dependent in the high frequency range (>60 Hz) .The exponential factor (s) values, which represent the slope of Ln(σ) versus Ln(ω) for the pure ppy and ppy/(MgO and $WO_3$) nanoparticle blends, were estimated according to equation (2) and listed in Table-1. It is clear that (**s**) values are greater than unity, which is due to the domination of a.c conductivity at high frequency range. It is obvious that (**s**) value for the pure PPy increases with temperature. Also, (s) increases when both oxides are added to the host polymer, which suggests that the CBH is the most stable model to explain our results. However, the results also showed that (s) decreases with further increase of doping ratio, which suggests that the SP model is suitable for composites samples. The Small Polaron Tunneling model is the most appropriate when the exponent (s) rises with the increase in temperature. The addition of the load carrier to the covalent solid induces a significant degree of local distortion of the lattice, which forms a small polaron. The increase of the exponent (s) values with rising the temperature suggests the reduction or the elimination of the defect states responsible for the adsorption of the gas. This suggests that gas sensitivity will be reduced with rising temperature, as will be shown later in this paper.

The results that are demonstrated in all figures show that the electrical conductivity of all grafted and non-grafted models changes slightly at low frequencies (confined between 10-100 Hz). Afterwards, it increases significantly at frequencies between $10^2$-$10^4$ Hz and then returns to a slight increase in the higher frequencies. This pattern of increase appears as if it is divided into three regions. The highest electrical conductivity was obtained from the model of ppy/0.01WO3 nanoparticle composite at the temperature of 323 K, and was equal to $3.67x10^{-1}$ $\Omega.cm^{-1}$. Also, the samples doped with $WO_3$ nanoparticles for all ratios showed a higher electrical conductivity compared with the undoped PPy and with ppy doped with different rates of MgO nanoparticles.

The use of tungsten oxide nanoparticles showed even more advantages, such as the spatial size reduction, which promotes a quantum confinement effect that significantly influences the transport of charges. These advantages also include the electronic band structure, and the large fraction of surface particle, and the increased surface-to-volume ratio, which provides more surface area for chemical and physical interactions [22]. The increase in the AC conductivity of PPy/(1 , 3, and 5 %) WO3

nanocomposites may be due to the increased mobility of electrons to high extended chain conformation in order to increase the probability of tunneling in all subsequent composites. It can also be attributed to the flexible semiconducting behavior of WO3.

Figures- (4, 5, and 6) show the plotting curves of ( $\varepsilon_r$) versus ln(ω) for pure ppy and ppy/(MgO and WO3) nanoparticle blends at different temperatures. The dielectric constant ($\varepsilon_r$) values of all samples were measured within the employed frequency range ($10^1$-$10^5$Hz). From the spectrum of ( $\varepsilon_r$ ) versus ln(ω), it is obvious that $\varepsilon_r$ tends to decrease with increased frequency, reaching lower values. This is because that the electrode blocking layer is regulated by the dielectric activity of the electrode polarization, whereas the dielectric signal at high frequency is not influenced by the polarization of the electrode.

Figures- ( 7, 8, and 9) show the plotting curves of ( $\varepsilon_i$) versus ln(ω) for pure ppy and ppy/(MgO and WO3) nanoparticle blends at different temperatures. The dielectric loss ($\varepsilon_i$) values of all samples tends to sharply decrease with increased frequency from 10 to 400 Hz, and returns to increase with increased frequency to up to maximum, before decreasing again. The relaxation time was calculated from frequencies corresponding to the dielectric loss maxima using the equation: $\omega = 1/\tau$ and the values of τ are listed in Table-5. The most significant result is that the location of the relaxation peaks is not affected strongly by the addition of nanoparticles, but obviously affected by changing temperature in an irregular manner.

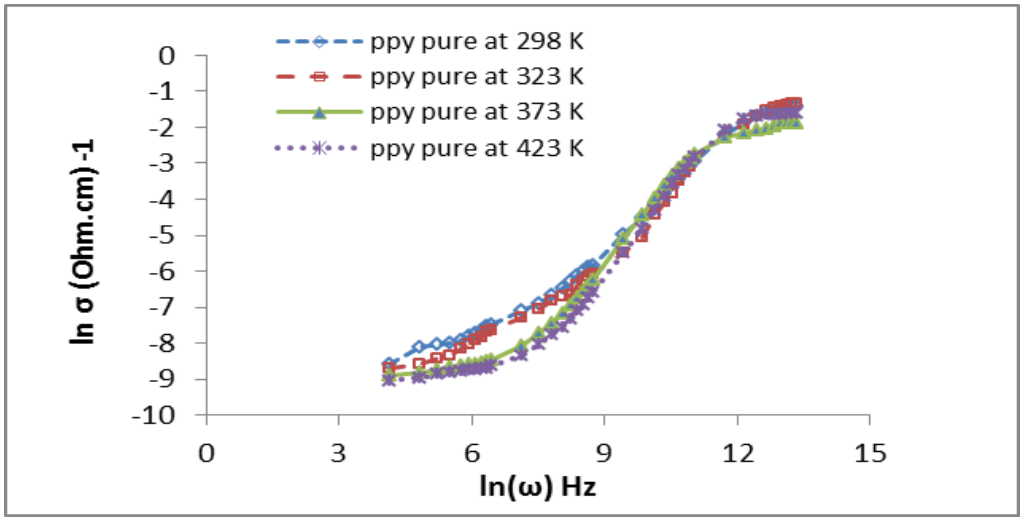


**Figure 1**-Ln $\sigma_{a.c}$ as a function of ln (ω) for PPy at different temperatures.

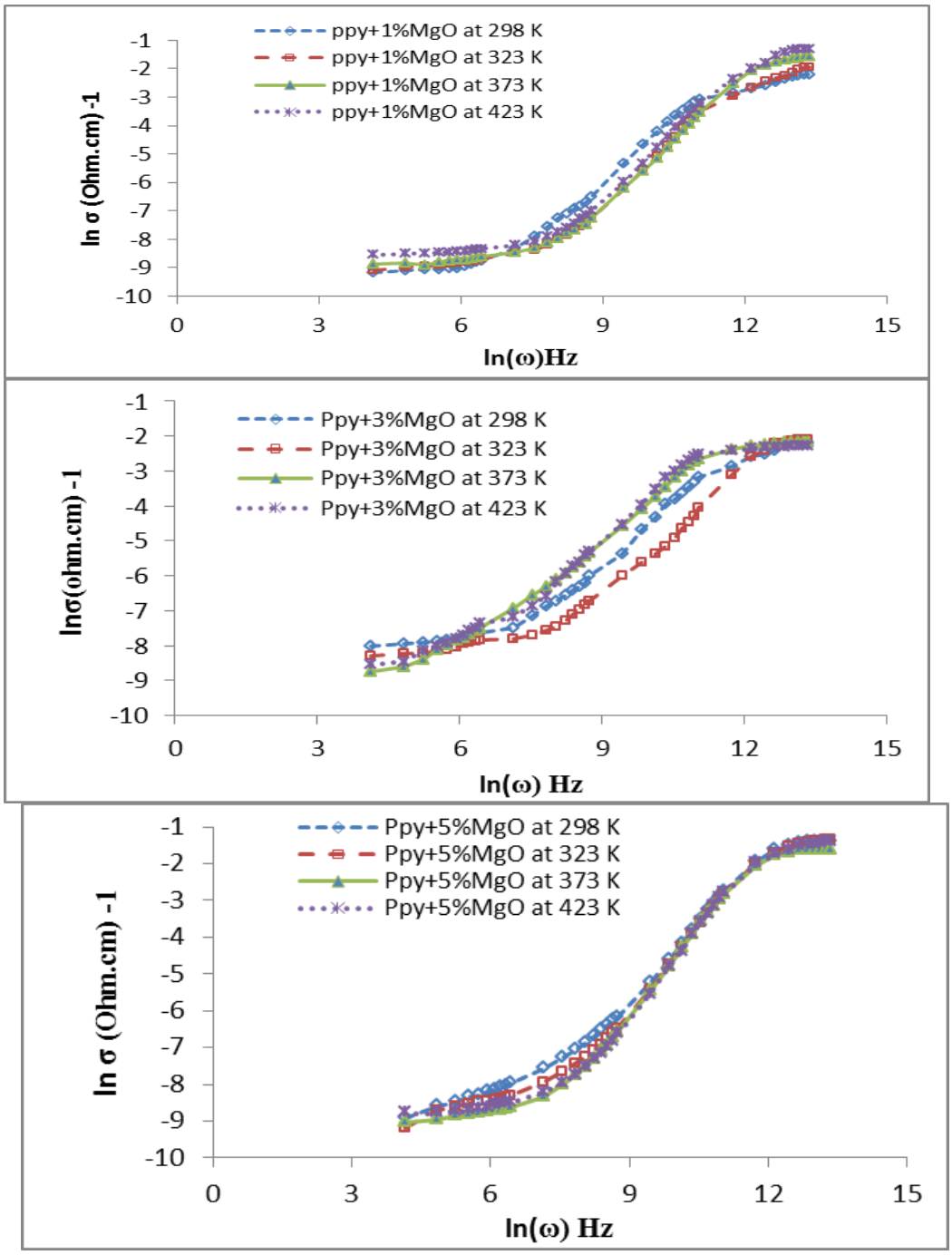


**Figure 2-**Ln $\sigma_{a.c}$ as a function of ln (ω) for PPy: 0.01,0.03 and 0.05 MgO composite.

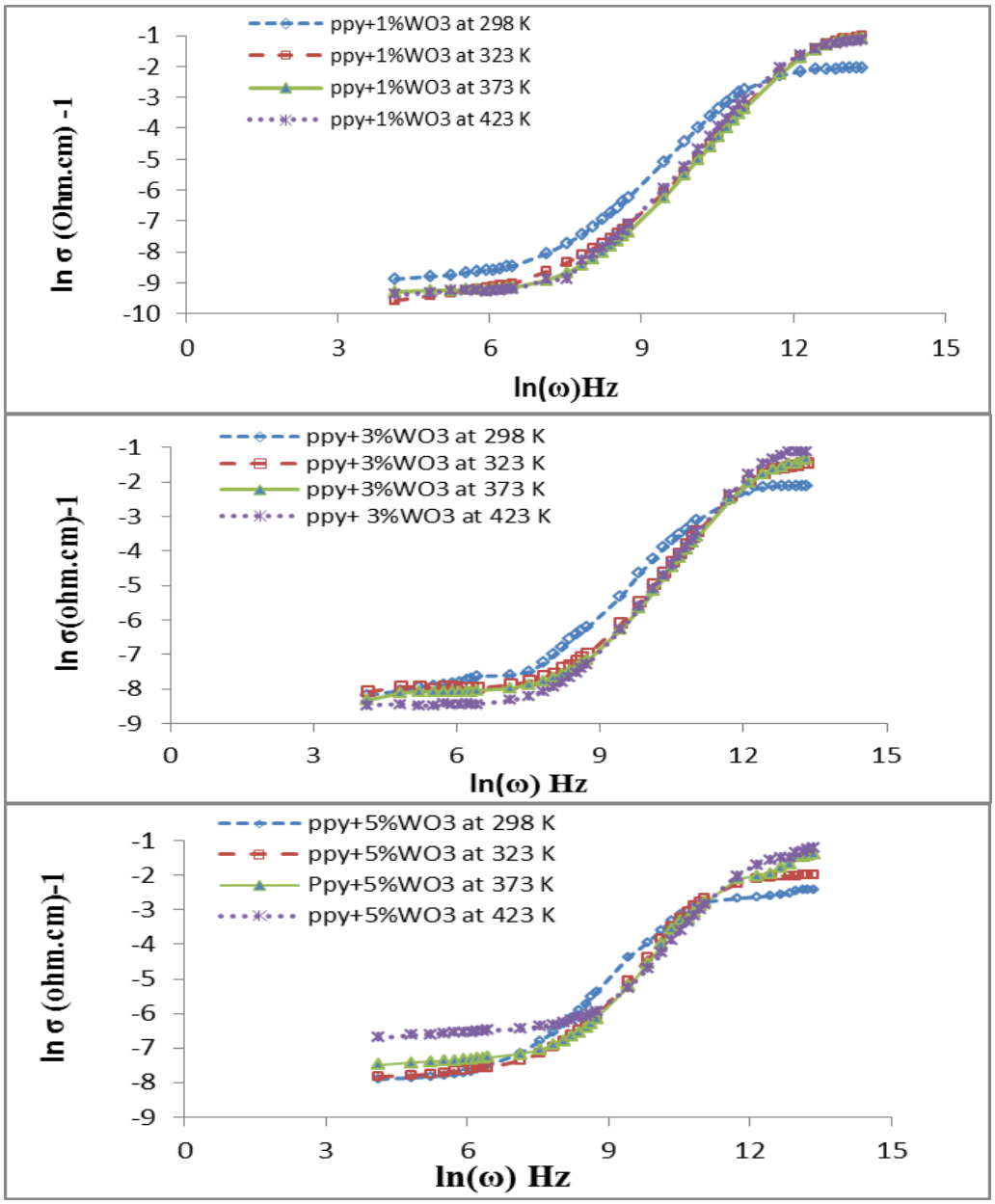


**Figure 3**-Ln $\sigma_{a.c}$ as a function of ln (ω) for PPy: (0.01,0.03 and 0.05 WO3) composite.

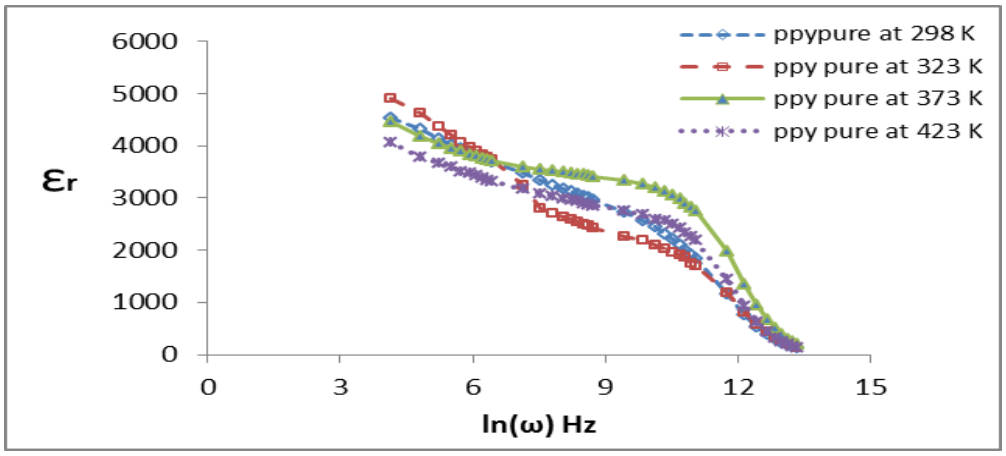


**Figure 4**- Real dielectric constant as a function of ln (ω) of pure PPy at different temperatures.

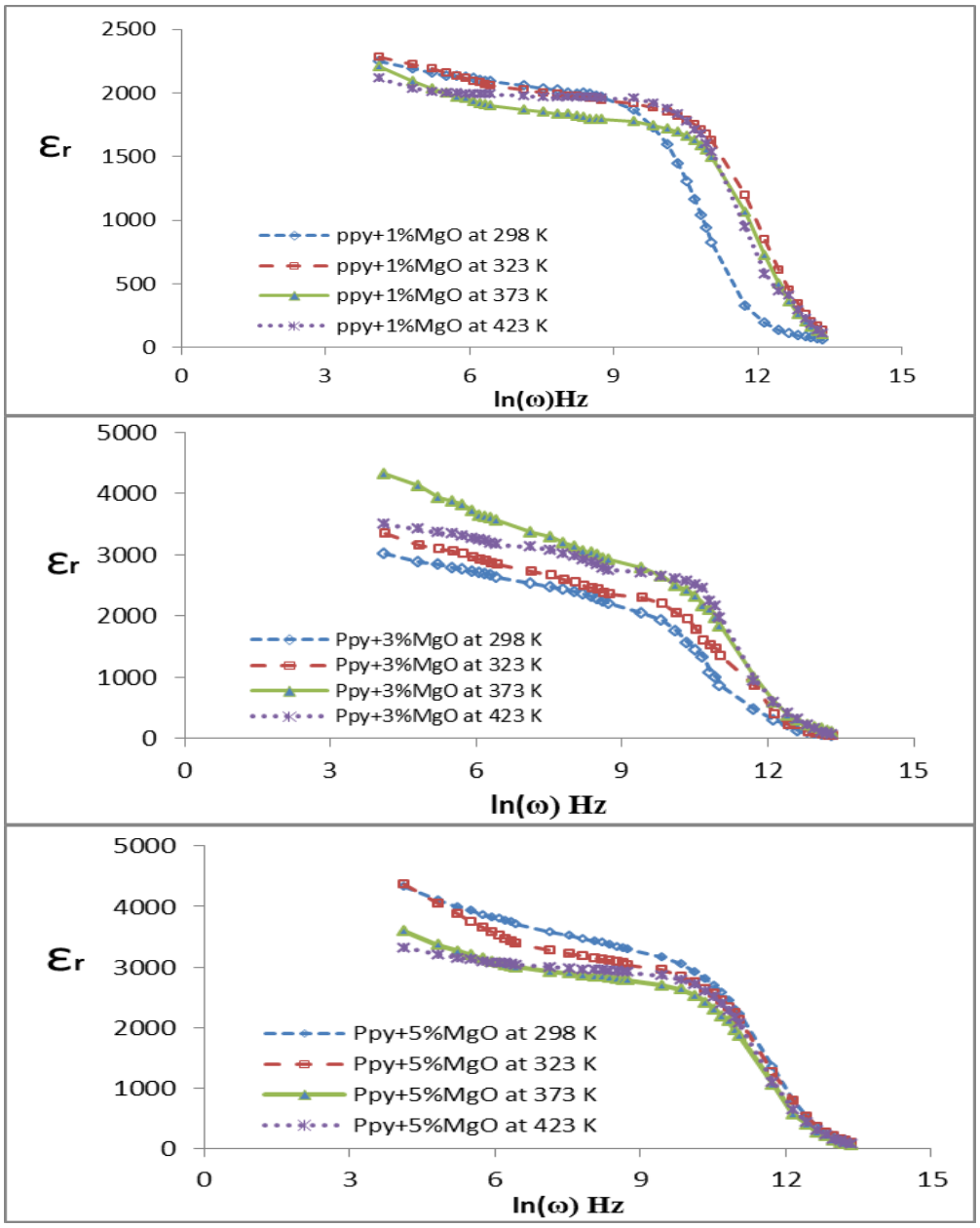


**Figure 5-** Real dielectric constant as a function of ln (ω) of PPy/(0.01,0.03 and 0.05 of MgO) composite at different temperatures.

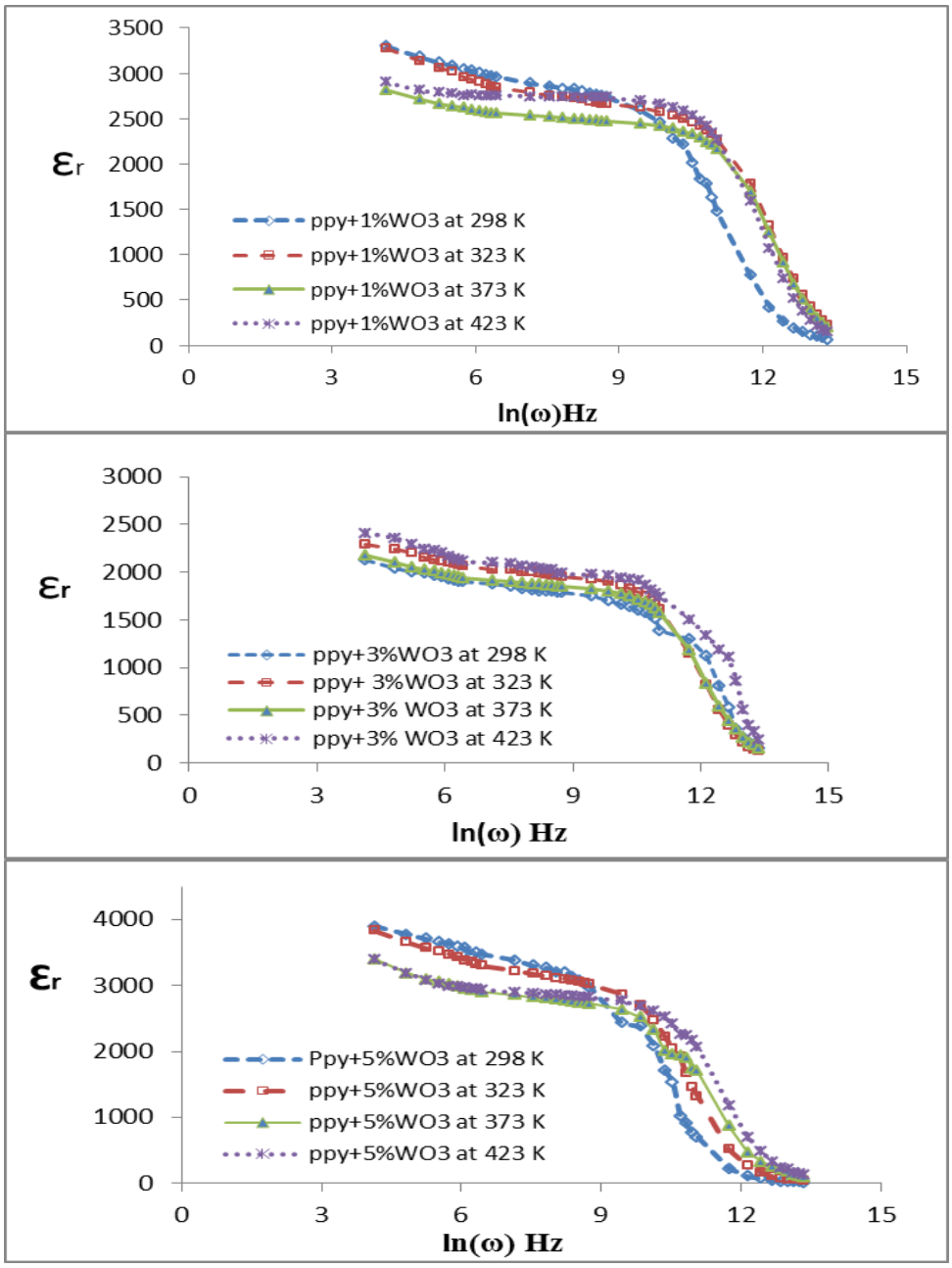


**Figure 6**-Real dielectric constant as a function of ln (ω) of PPy/(0.01,0.03 and 0.05) of $WO_3$ composite at different temperatures.

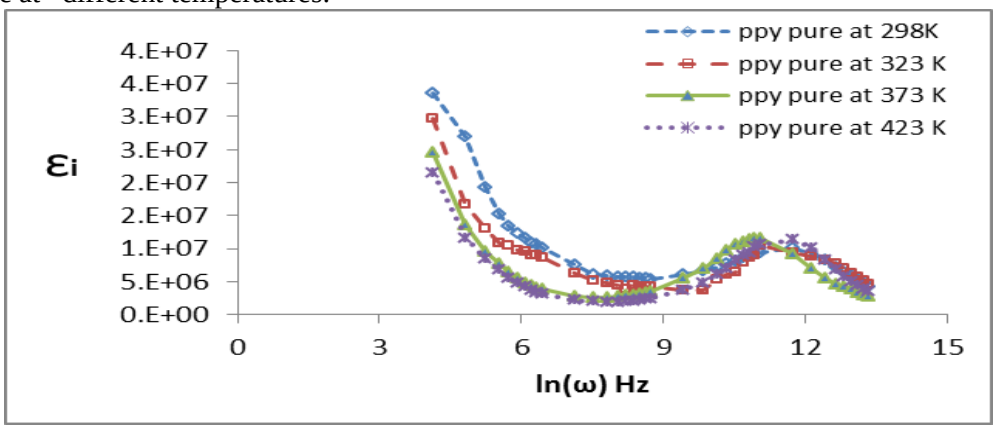


**Figure 7-** Imaginary dielectric constant as a function of ln (ω) of pure PPy at different temperatures.

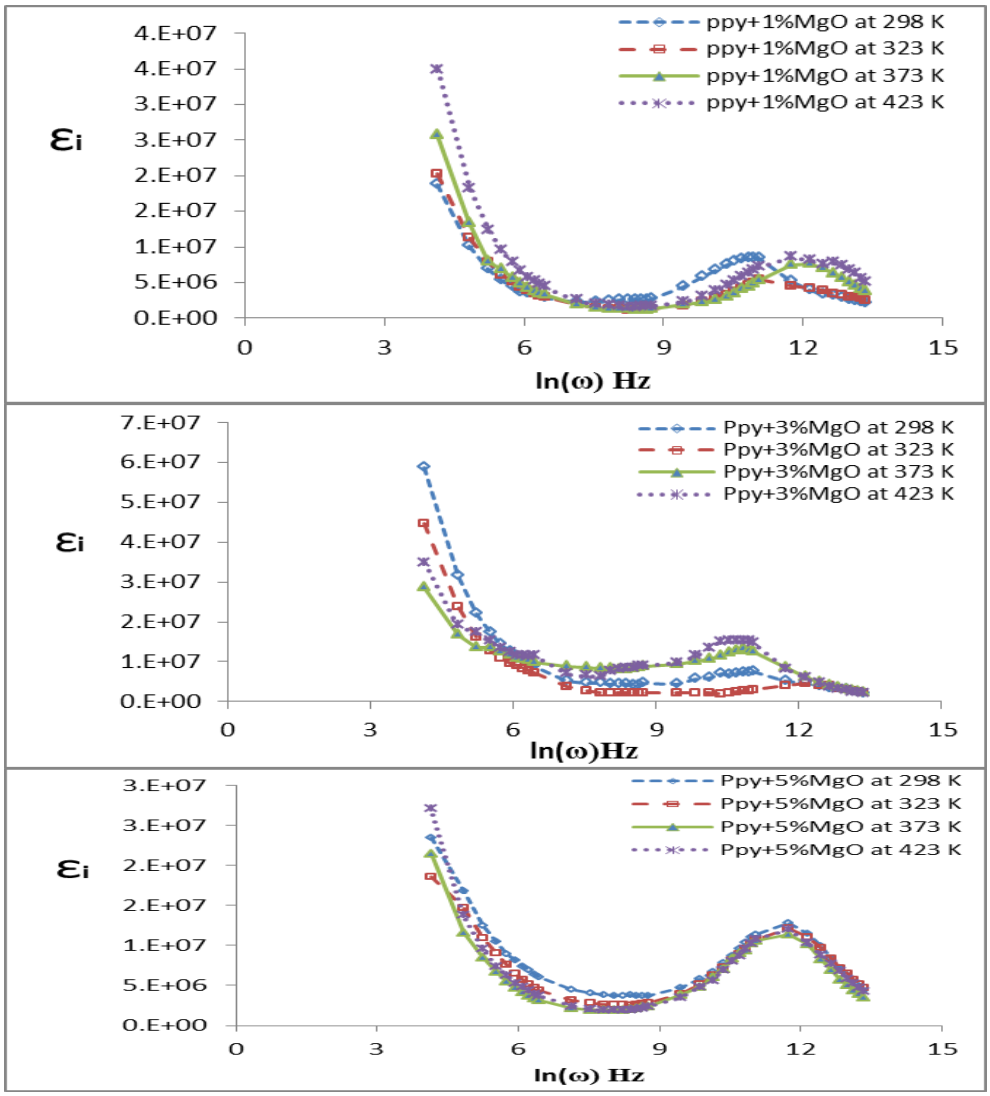


**Figure 8**- Imaginary dielectric constant as a function of ln (ω) of PPy/(0.01,0.03 and 0.05) of MgO composite at different temperatures.

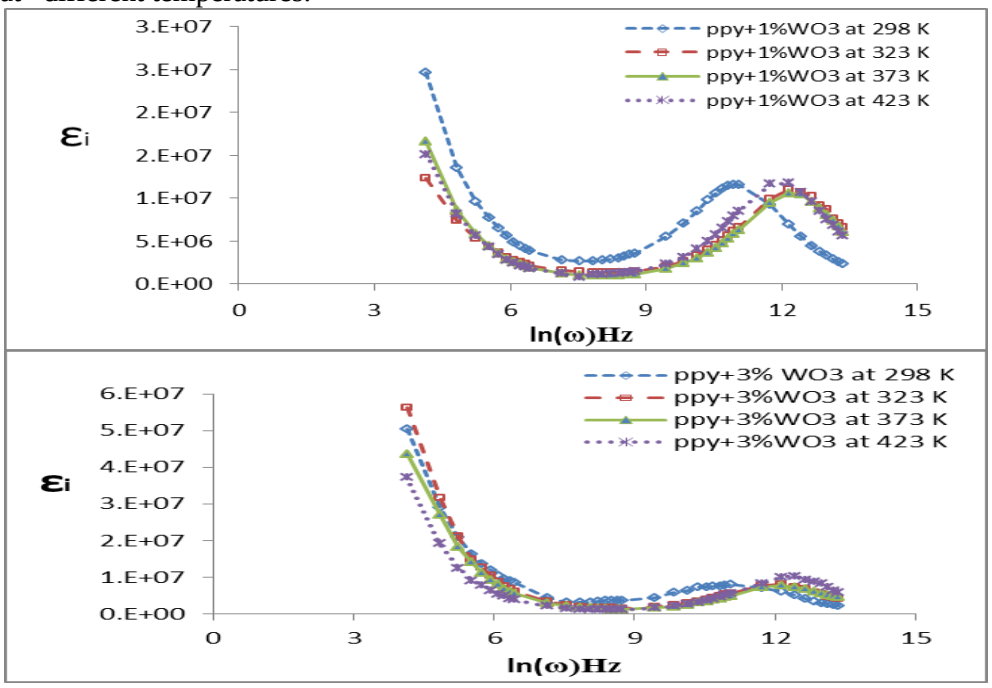

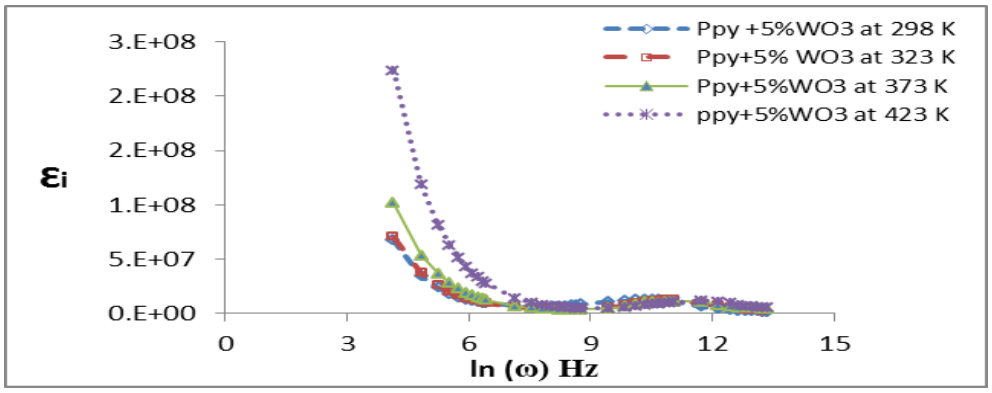


**Figure 9**-Imaginary dielectric constant as a function of ln (ω) of PPy/(0.01,0.03 and 0.05 of WO3) composite at different temperatures.

**Table 1**-The values of s of for pure and MgO and $WO_3$ doped PPy at different temperatures. .

| Type of sample | Blend Percentage | (s) at 298 K | (s) at 323K | (s) at 373K | (s) at 423K |
|---|---|---|---|---|---|
| ppy | 0% | 1.28 | 1.666 | 1.47 | 1.62 |
| Ppy+ MgO | 1% | 1.56 | 1.666 | 1.61 | 1.666 |
| | 3% | 1.22 | 1.315 | 1.316 | 1.22 |
| | 5% | 1.54 | 1.62 | 1.62 | 1.666 |
| Ppy+WO3 | 1% | 1.56 | 1.714 | 1.666 | 1.786 |
| | 3% | 1.333 | 1.579 | 1.666 | 1.666 |
| | 5% | 1.316 | 1.666 | 1.6 | 1.5 |

**Table 2**-The values of $\tau$ of undoped PPy and that doped with MgO and WO3 for different concentrations and at different temperatures.

| Type of sample | Blend Percentage | $\tau$ (Sec) at 298K | $\tau$ (Sec) at 323K | $\tau$ (Sec) at 373K | $\tau$ (Sec) at423K |
|---|---|---|---|---|---|
| ppy | 0% | $7.96x10^{-6}$ | $1.59x10^{-5}$ | $1.77x10^{-5}$ | $7.96x10^{-6}$ |
| ppy + MgO | 1% | $1.77x10^{-5}$ | $1.59x10^{-5}$ | $5.31x10^{-6}$ | $7.96x10^{-6}$ |
| | 3% | $1.59x10^{-5}$ | $5.3x10^{-6}$ | $1.99x10^{-5}$ | $1.77x10^{-6}$ |
| | 5% | $7.96x10^{-6}$ | $7.96x10^{-6}$ | $7.96x10^{-6}$ | $7.96x10^{-6}$ |
| ppy + WO3 | 1% | $1.77x10^{-5}$ | $5.3x10^{-6}$ | $5.3x10^{-6}$ | $5.3x10^{-6}$ |
| | 3% | $1.59x10^{-5}$ | $5.3x10^{-6}$ | $5.3x10^{-6}$ | $3.98x10^{-6}$ |
| | 5% | $2.65x10^{-5}$ | $1.77x10^{-5}$ | $1.59x10^{-5}$ | $7.96x10^{-6}$ |

To record the response to ammonia gas, the pure and MgO- and $WO_3$-doped PPy nanocomposite film sensors deposited on the ITO glass substrate were further used for sensor applications. Figures-10 to 16 show the results of resistance, as a function of time at room and other working temperatures, for the pure PPy, PPy doped with 0.01, 0.03 and 0.05 MgO, and PPy doped with 0.01, 0.03 and 0.05 $WO_3$, respectively. As the $NH_3$ gas is fed into the chamber, the sensor resistance keeps rising. This behavior is related to the semiconductor's p-type form. The decrease in the resistance of the sensor that is observed under synthetic air exposure is consistent with the desorption of ammonia molecules from the polypyrrole film. It is well known that the exposure of PPy to reducing gases, like NH3 gas which is considered as an electron-donating gas, reduces the conductivity. The conductivity of MgO and WO3-doped PPy are volatile to NH3, as a redox (dedoping) reaction can rapidly occur. The charge transfer between the electron-donating reducing NH3 gas and PPy, which is p- type, results in the formation of neutral polymer chains, which consequently decreases the charge carriers density . On the other side , the adsorption of NH3 molecules on PPy films reduces the number of holes in PPy and thus increases resistance [23].

The sensitivity value of pure PPy, estimated from applying equation (10), is equal to 126.3 %, while it decreases non-systematically when with rising working temperature. The results of variation in response time and recovery time for pure PPy and that doped with MgO and WO3 at different working temperatures are shown in Tables- 4 and 5, respectively. It can be observed that both parameters change in a nonsystematic manner for different materials with the rising of operating temperature; (i.e. the response time increases and then decreases for the pure PPy, whereas it decreases and then increases for the doped samples. However, the recovery time decreases and then increases for pure PPy, whereas it increases and then decreases for the doped samples.

Carquigny *et al*. have already studied the mechanism of contact between a polymer film and ammonia [24]. Since polypyrrole can be considered as a p-type semiconducting material composed of both neutral and oxidized monomer units, ammonia adsorption on PPy films was shown, in the beginning, to lose electron by doubling some polymer backbone nitrogen atoms, resulting in the formation of $NH^+$ radical groups. This transfer of electron between the ammonia molecule and the positive hole of the polymer induces a decrease in the positive charge density, which results in an increase in the resistance. Consequently, the polymer becomes less conductive after adsorption of $NH_3$, and the measured resistance increases. On the contrary, the sensor's resistance decreases during the desorption of ammonia molecules [25]. The plot diagrams shown in Figures- 11 to 16 show the results of resistance as a function of time for the MgO and WO3 doped Ppy gas sensor cells at different temperatures . It is clear that the sensor cells still exhibit p-type, since the resistance grows upon the sensors' exposure to $NH_3$ gas, and return to the original values as the gas is removed. It is also clear that sensitivity values of sensors at elevated temperatures are lower than that obtained at room temperature. This result is similar to the findings of other researchers [26], which confirm that the polymer base sensors are room temperature types of gas sensors. One can observe from Table-3 that the highest sensitivity values toward $NH_3$ were achieved at room temperature for all doping ratios (0.01, 0.03, and 0.05) of both nanoparticles used in this work, while the sensitivity decreased by rising the working temperature and reached a minimum value of 21.63% at 0.01%$WO_3$ NPs and a temperature of 423 K.

Another observation is that the resistance of the composite increases during the exposure to $NH_3$ gas for some seconds and, when it reaches the point of saturation, the increase in resistance stops as a result of the cessation of the film's interaction with the gas. When the gas is cut off from the room, the resistance begins to gradually decrease until it returns to the original value before exposure to the gas, which takes longer time compared to the response time. Testsuya and Koroiwa [27] pointed out that the response speed of a sensor device based on a SnO2 porous film (pore size at maximum population: 37nm) was remarkably high, reaching a response time of less than 1s for $H_2$ and CO detection at 250 and 350 °C. This suggests that the diffusion and surface reaction of $H_2$ and CO are quite fast in the porous film. On the other hand, they found that the recovery speed was not comparably fast and the resistance of the device did not recover to the original state within 20s after switching the gas atmosphere in the chamber from the sample gases to air. This is possibly due to the slow desorption of the $H_2O$ and $CO_2$ that were formed by the surface reaction of $H_2$ and CO, respectively, with the adsorbed oxygen on $SnO_2$.

It is worth remarking that the sensitivity decreases as the dopant metal oxides were introduced to the host polymer, i.e. the sensitivity decreases from 126 % to 35.75 % at PPy/0.03%MgO and to 62.02 % at PPy/0.01%WO3, but then grows to 104.95% and 143.25 % for PPy/0.05 % MgO and PPy/0.03 % WO3 gas sensors, respectively. The interesting results are that the maximum sensitivity is obtained at room temperature and a significant reduction of the sensitivity values occurs at elevated working temperatures (Table-3). The sensitivity value obtained can be attributed to that $WO_3$ is an n-type semiconductor material with a wide energy band gap varying in the range from 2.6 to 3.25 eV [28], its baseline resistances is higher, and its device resistance drops more significantly in general and, hence, its sensing response is much higher. Therefore, the ppy/$WO_3$ sensor processes the strongest response signal [29]. From the results shown in Table-4, we find that the fastest response time is equal to 16 sec at 423 K for pure PPy, whereas the slowest response time recorded (34 sec) is at 298 K for PPy/0.01 WO3. In general, we found that the response time recorded at testing for the majority of samples at different temperatures is confined between 16 to 34 sec. From another side, the recovery time was found to change in response to the temperature and weight percentage, as seen in Table-4. Figure-17 shows the relation between sensitivity and working temperature for undoped and doped PPy .

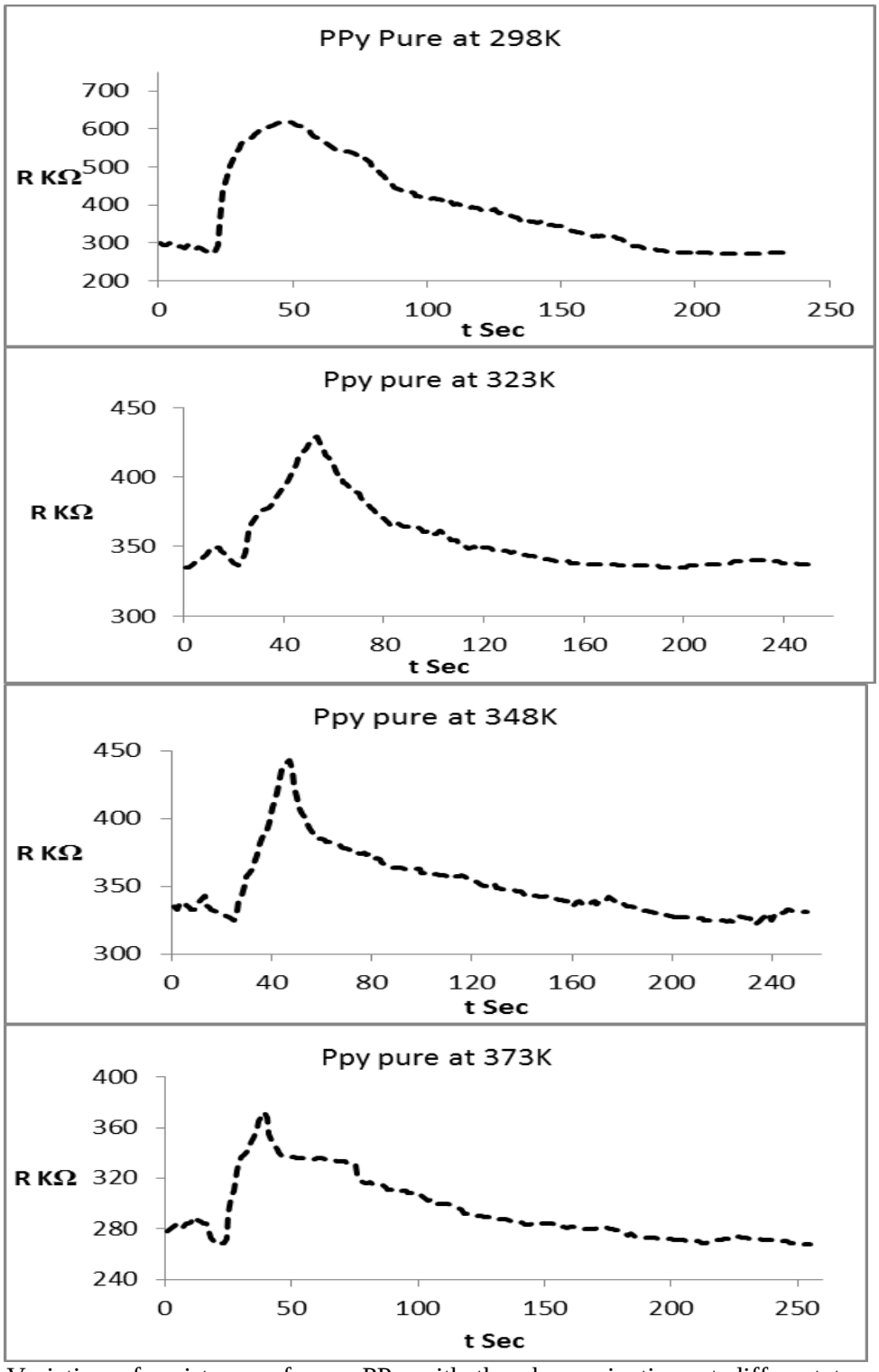


**Figure 10**-Variation of resistance of pure PPy with the change in time at different temperatures.

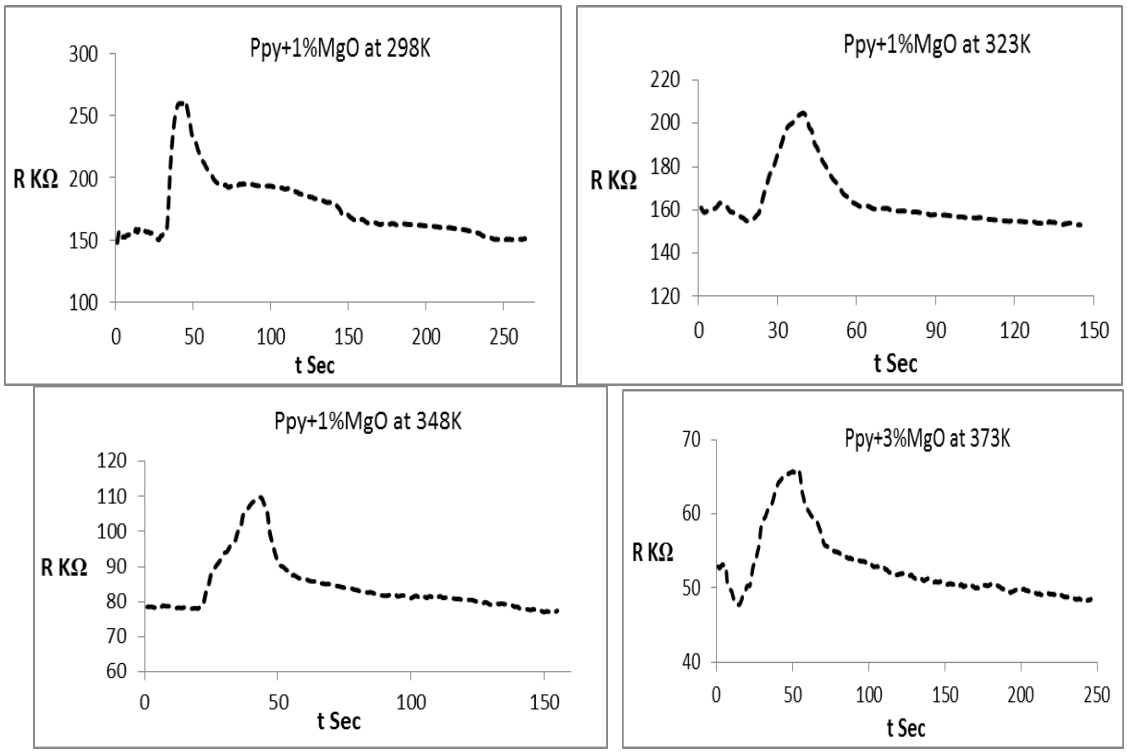


**Figure 11-** Variation of resistance of PPY/ 0.01MgO with change in time at different temperatures.

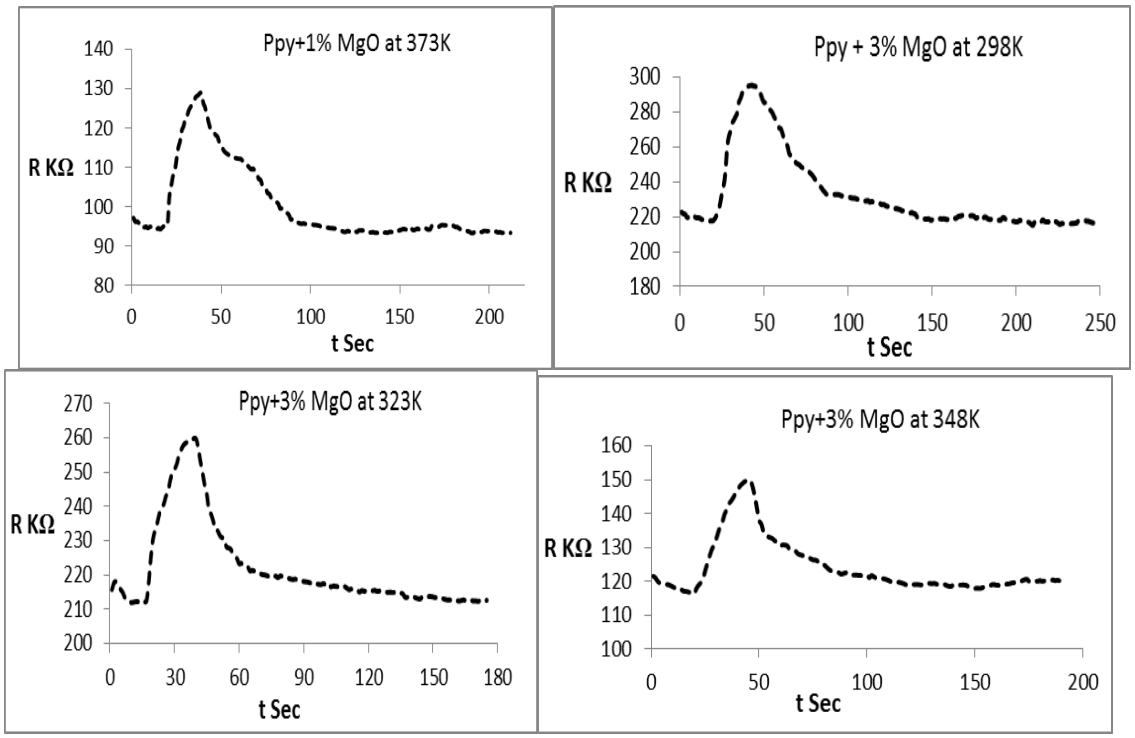


**Figure 12** - Variation of resistance of PPY/ 0.03MgO with change in time at different temperatures.

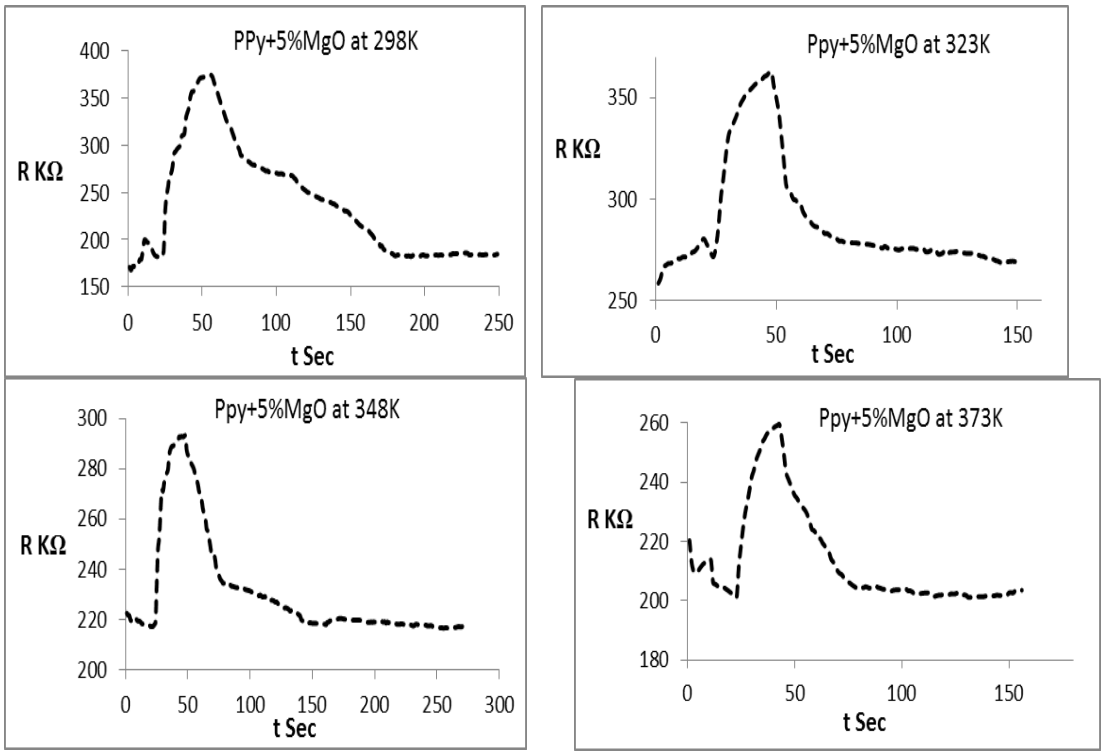


**Figure** 13-Variation of resistance of PPY/ 0.05MgO with change in time at different temperatures.

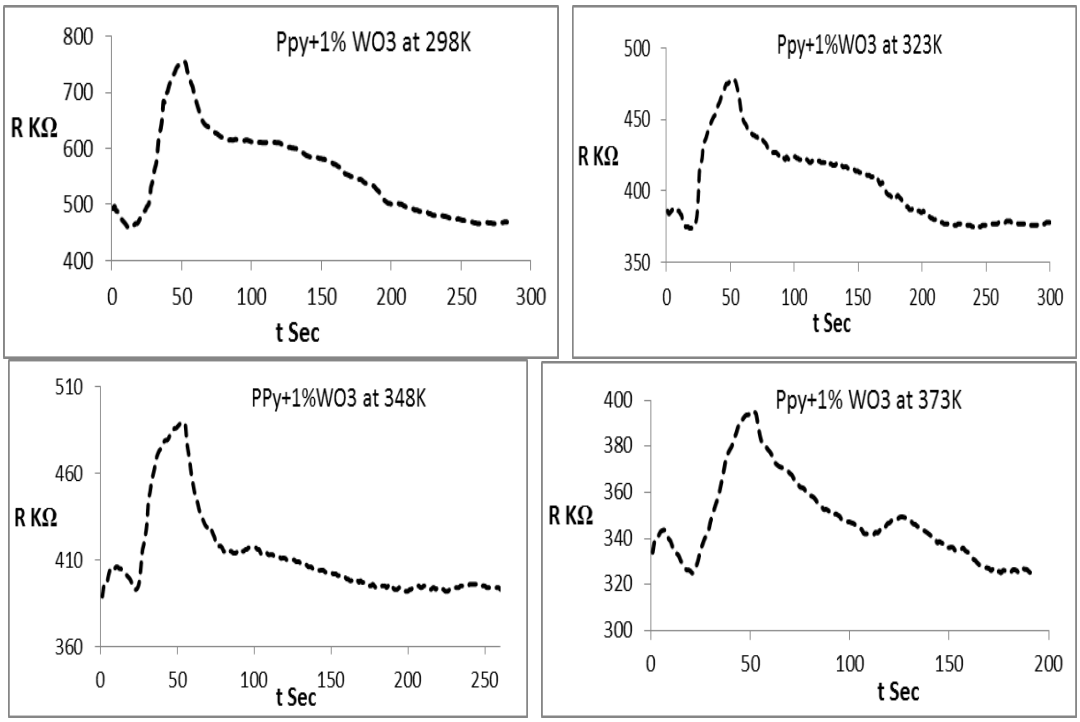


**Figure 14 -** Variation of resistance of PPy doped with 0.01 WO3 with time at different temperatures .

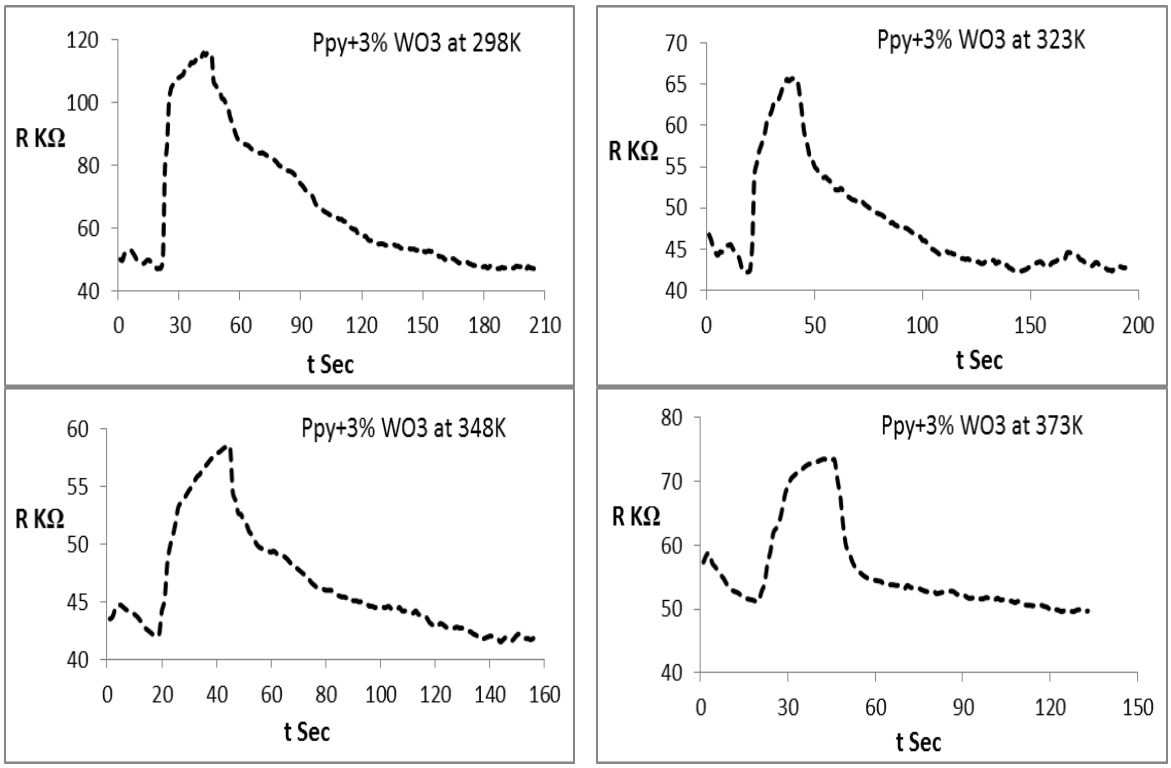


**Figure 15** -Variation of resistance of PPy doped with 0.03 WO3 with time at different temperatures .

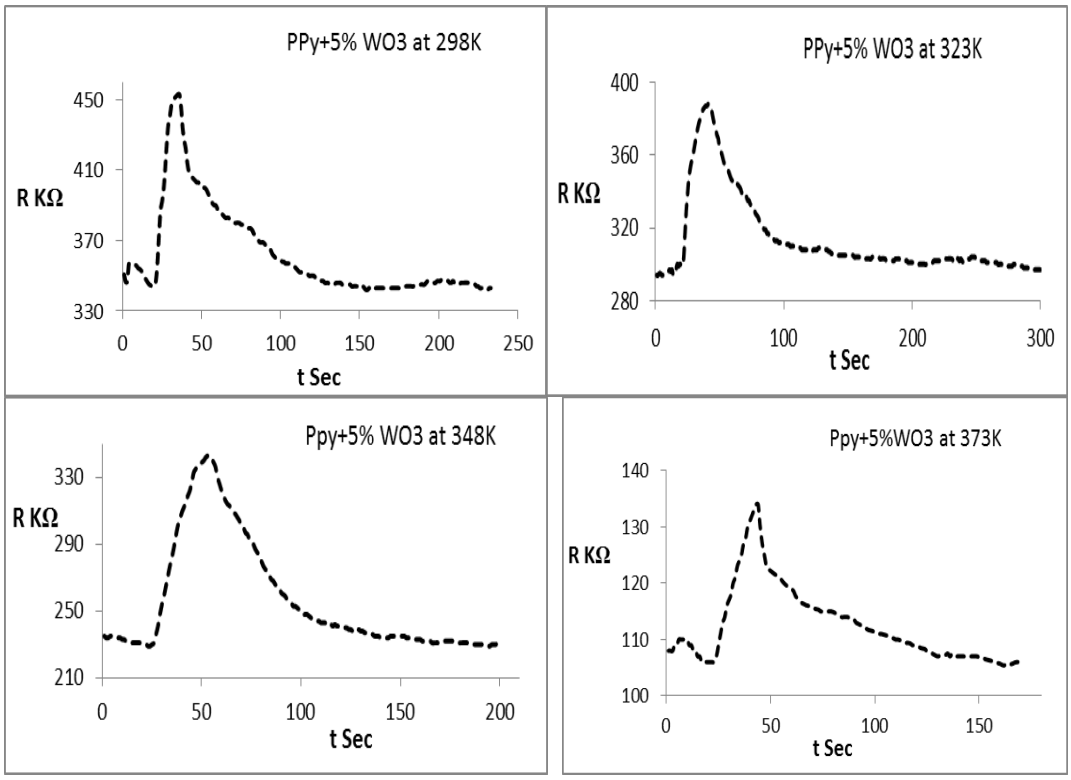


**Figure 16 -** Variation of resistance of PPy doped with 0.05 WO3 with time at different temperatures

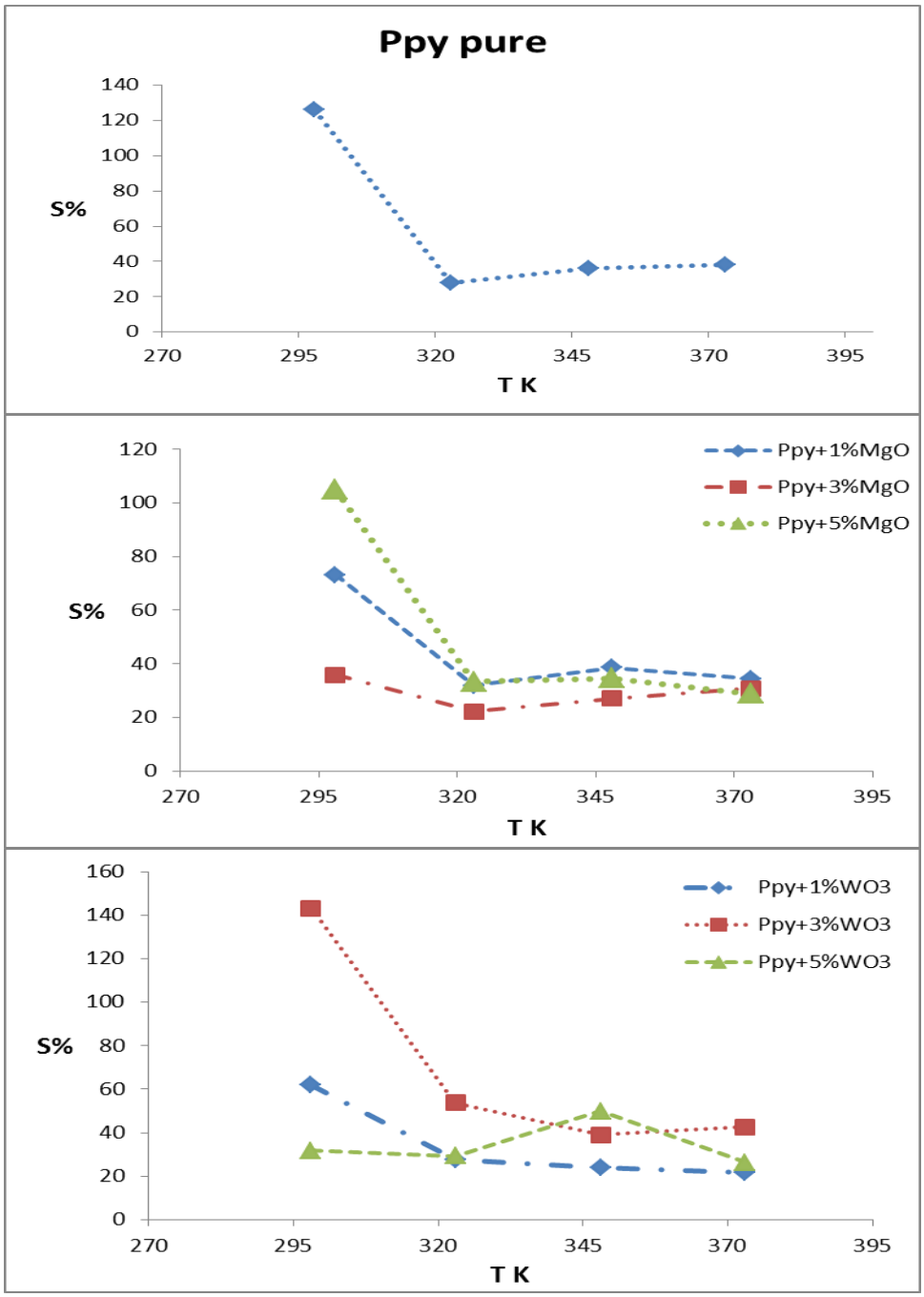


**Figure 17**-The sensitivity (S%) as a function of working temperature of PPy (undoped and doped with MgO and $WO_3$).

Table **3**-The sensitivity of PPy (pure and doped) nanoparticles upon exposure to ammonia gas.

| Type of sample | Blend Percentage | S% at 298K | S % at 323K | S % at 373K | S % at 423K |
|---|---|---|---|---|---|
| PPy pure | 0% | 126.3 | 27.67 | 36.31 | 38.28 |
| PPy + MgO | 1% | 73.09 | 31.9 | 38.55 | 34.45 |
| | 3% | 35.75 | 22.27 | 26.97 | 30.75 |
| | 5% | 104.93 | 33.38 | 34.49 | 28.92 |
| PPy + WO3 | 1% | 62.02 | 27.54 | 24.17 | 21.63 |
| | 3% | 143.25 | 53.81 | 38.95 | 42.69 |
| | 5% | 31.68 | 29.33 | 49.78 | 26.41 |

**Table 4**-The response time of pure and doped PPy nanoparticles at various temperatures upon exposure to ammonia gas.

| Type of sample | Blend Percentage | t (sec) at 298K | t (sec) at 323K | t (sec) at 373K | t (sec) at 423K |
|---|---|---|---|---|---|
| PPy pure | 0% | 19 | 31 | 22 | 16 |
| PPy+MgO | 1% | 17 | 20 | 22 | 19 |
| | 3% | 25 | 23 | 25 | 32 |
| | 5% | 33 | 24 | 25 | 20 |
| PPy+WO3 | 1% | 34 | 33 | 32 | 30 |
| | 3% | 24 | 21 | 25 | 25 |
| | 5% | 17 | 22 | 30 | 21 |

**Table 5-**The recovery time of pure and doped PPy nanoparticles at various temperatures upon exposure to ammonia gas

| type of sample | Blend Percentage | t (sec) at 298K | t (sec) at 323K | t (sec) at 373K | t (sec) at 423K |
|---|---|---|---|---|---|
| PPy pure | 0% | 148 | 121 | 166 | 173 |
| PPy+MgO | 1% | 158 | 75 | 86 | 65 |
| | 3% | 153 | 122 | 104 | 104 |
| | 5% | 130 | 88 | 113 | 87 |
| PPy+WO3 | 1% | 210 | 187 | 136 | 123 |
| | 3% | 136 | 101 | 90 | 61 |
| | 5% | 109 | 162 | 139 | 114 |

## 4- Conclusions

From this work, several points may be concluded. *In situ* electrochemical polymerization produced homogeneous PPy films with a thickness that is nearly at the micrometer scale. The highest a.c conductivity value of $3.67x10^{-1}\ \Omega.cm^{-1}$ was obtained for the PPy doped with WO3, which exceeded that for the pure PPy and that doped with MgO. Good correlation was obtained between the exponent factor (s) and the most sensitive gas sensors cell , i.e. a high sensitivity value was obtained when the (s) value was in a range $\leq 1.5$ , whereas a high (s) value accompanied low sensitivity.

Rising the operating temperature caused a reduction in sensitivity. Increased temperature caused an increase $\varepsilon_r$ value for PPy with low doping ratio of MgO (1 and 3%). The opposite occurred with the high doping ratio. However, the addition of $WO_3$ caused an increase in $\varepsilon_r$ for all doping ratios. The addition of both types of nanoparticles had no effect on the location of the relaxation peaks in $\varepsilon_i$ spectra .

The sensitivity measurement performed in the presence of ammonia flow showed interesting sensitivity responses (126.7 % for pure PPy and 143.25% for PPy+3 % $WO_3$) with good reproducibility. By comparison with most of chemiresistor gas sensors, our PPy-based sensor confers best sensitivity at room temperature.

## References

**1.** Hua Bai and Gaoquan Shi. **2007.** Gas Sensors Based on Conducting Polymers**,** *Sensors,* **7**: 267-307.

**2.** J.H. Burroughes, D.D.C. Bradley, A.R. Brown, R.N. Marks, K. MacKay, R.H. Friend, P.L. Burns and A.B. Holmes, **1990.** Lightemitting diodes based on conjugated polymers, *Nature,* **347**: 539-541.

**3.** Tilia Patois, Jean-Baptiste Sanchez, Franck Berger, Jean-Yves Rauch, Patrick Fievet, Boris Lakar, **2012**. Ammonia gas sensors based on polypyrrole films: Influence of electrodeposition parameters, *Sensors and Actuators B*, **171–172**: 431–439.

**4.** D.L. Wise, G.E. Wirek, D.J. Trantolo, T.M. Cooper and D. Gresser, **1998**. Electrical and Optical Polymer Systems, *Poly. Int*., **49**: 316-318.

**5.** Q. Ameer, S. B. Adeloju. **2005.** Polypyrrole-based electronic noses for environmental and industrial analysis, *Sens. Actuators B*, **106**: 541–552.

**6.** K. Arora, A. Chaubey, R. Singhal, R.P. Singh, M.K. Pandey, S.B. Samanta, B.D. Malhotra, S. Chand, **2006**. Application of electrochemically prepared polypyrrole–polyvinyl sulphonate films to DNA biosensor, *Biosens. Bioelectron*. **21**: 1777–1783.

**7.** Sen, T., Mishra S. and Shimpi N.G. **2016**. Synthesis and sensing applications of polyaniline nanocomposites. *A review*. *RSC Adv*. **6**: 42196–42222.

**8.** Orzani E.S., Li X. and Tao N. **2007**. Hybrid amperometric and conductometric chemical sensor based on conducting Polyme nanojunctions, *Anal. Chem*. **79**: 5217–5224.

**9.** M. Penza, E. Milella, M.B. Alba, A. Quirini, L. Vasanelli, **1997.** Selective NH3 gas sensor based on Langmuir–Blodgett polypyrrole film, *Sens. Actuators B*, **40**: 205–209.

**10.** Geng L, Zhao Y, Huang X, Wang S, Zhang S, Wu S. **2007**. Characterization and gas sensitivity study of polyaniline SnO2 hybrid material prepared by hydrothermal route, *Sensors Actuators B* **120**: 568–572.

**11.** Kwon, O.S.; Hong, J.Y.; Park, S.J.; Jang, Y.; Jang, J. **2010**. Resistive gas sensors based on precisely size-controlled polypyrrole nanoparticles: Effects of particle size and deposition method, *J. Phys.Chem*.**114**: 18874–18879.

**12.** Seon J. P., Chul S. P. and Hyeonseok Y. **2017**. Chemo-Electrical Gas Sensors Based on Conducting Polymer Hybrids, *Polymers*, **9**: 155.

**13.** S.R .Elliot,**1987**. A.c. Conduction in Amorphous Chalcogenide and Pnictide Semiconductors, *Adv. In. Phys*., **36**(2): 135.

**14.** Smyth, C. P.**1955**.*Dielectric Behavior and Structure*, New York . McGraw-Hill.

**15.** Mott, N. F. and Davis, E. A. **1971**. *Electronic Processes in Non-Crys. Materials*, New York. Oxford University Press.

**16.** R. Singh, A.K. Narula, R.P. Tandon, A. Mansigh and S. Chandra,**1996.** Mechanism of charge transport in polypyrrole, poly (N-methyl pyrrole) and their copolymers**,** *J. Appl. Phys*, **79**: 1476-1480.

**17.** Omer, M. A. **1973.** *Elementary Solid State Physics*, 1st edition, Wesly Pub. Co.

**18.** T. K. Vishnuvardhan, V. R. kulkarni, C. Basavaraja, S. C. Raghavendra. Bull.Mater. **2006**. Synthesis, characterization and a.c. conductivity of polypyrrole/Y 2 O 3 composites, *Bulletin of Materials Science*, **29**(1): 77-83.

**19.** S. Sagadevan, J. Podder, **2015**. Optical and Electrical Properties of Nanocrystalline SnO 2 Thin Films Synthesized by Chemical Bath Deposition Method ,*Soft Nanoscience Letters*, **5**: 55-64.

**20.** Sara S. Mahmood, and Bushra A. Hasan, **2018.**Characterization of $(SnO2)_{1-x}$ $(TiO2:CuO)_x$ films as NH3 gas sensor, *Iraqi Journal of Physics*,**16**(39): 71-80.

**21.** A. Yang, **2008**. "Gas Sensors Made from Electrospun Nanofibers Doped by Functionalized Carbon Nanotubes" PhD thesis, The Hong Kong Polytechnic University, Institute of Textiles and Clothing.

**22.** Ana Marques, Lídia Santos, Sónia Pereira, Umberto Emanuele, Stefano Sinopoli, RuiIgreja, Goreti Sales, Rodrigo Martins and Elvira Fortunato, **2018**. A Planar Electrochromic Device using WO3 Nanoparticles and a Modified Paper-Based Electrolyte, *Proceedings*, **2**(13): 1065-1069.

**23.** Anil G. Sonkusare1, Sachin Tyagi, Sunita Mishra, Mamanpreet Kaur, Ranjan Kumar ,**2018**. Ammonia sensing using conducting polymer Ploypyrrole-coated silicon wafer, *International Journal of Applied Environmental Sciences*, **139**(1): 59-69.

**24.** Carquignya S, Sanchez J -B, Berger F, Lakard B and Lallemand F. **2009**. *Ammonia Gas Sensor Based on Electrosynthesized Polypyrrole Films*, Talanta, Elsevier, **78**(1): 199-206.

**25.** K J Dunst, K Cysewska, P Kalinowski, P Jasiński, **2015**. Polypyrrole based gas sensor for ammonia detection, *Materials Science and Engineering*, **104**(1).

**26.** N. Karmakara, R Fernandesa , Shilpa Jainb, U.V.Patilc, Navinchandra G.Shimpib, N.V. Bhatd, D.C. Kotharia, **2017**. Room temperature NO2 gas sensing properties of p-toluenesulfonic acid doped silver-polypyrrole nanocomposite, *Sensors and Actuators B Chemical*, **242**: 118-126.

**27.** 27- Tetsuya Kida, Toru Kuroiwa, Masayoshi Yuasa, Kengo Shimanoe, Noboru Yamazoe, **2008.** Study on the response and recovery properties of semiconductor gas sensors using a high-speed gas-switching system, *Sensors and Actutaors B chemical*, **134**(2): 928-933.

**28.** W.L. Kwong, N. Savvides, C.C. Sorrell,**2012**. Electrodeposited nanostructured WO3 thin films for photoelectrochemical application, *Electrochimica Acta*, **75**: 371–380.

**29.** A.T. Manea, S.T. Navalea, R.C. Pawarb, C.S. Leeb, and V.B. Patila. **2015**. Microstructural, optical and electrical transport properties of WO3 nanoparticles coated polypyrrole hybrid nanocomposites, *Synthetic Metals*, **199**: 187-195.